CIMAC CONGRESS 25
ZURICH, MAY 19 – 23, 2025

2025 | 042

Dynamics of the high-pressure hydrogen jet using high-speed Schlieren and Optical Flow Estimation

Fuel Injection & Gas Admission and Engine Components

Qiang Cheng, Aalto University

Maryam Yeganeh, Aalto University
Jennifer Schurr , Aalto University
Chao Yang, Aalto University
Ville Vuorinen , Aalto University
Ossi Kaario, Aalto University

ABSTRACT

Hydrogen (H2) as a carbon-free fuel and its excellent combustion properties has been extensively attracted the interest for utilizing H2 as a energy career to replace the conventional fossil fuels in internal combustion engines (ICEs) application. Accordingly, the primary focus of this study is to investigate the dynamics of the non-reactive H2 jet with different nozzles and operating conditions, which is crucial for fuel/air mixing in direct injection (DI) engines. High-speed z-type Schlieren imaging is employed in a constant volume chamber to study the effect of nozzle geometry (out-ward opening, single-hole) and pressure ratio (PR= injection pressure/chamber pressure) on the H2 jet characteristics. To gain an insight into the velocity field of the dynamics of the H2 jet, an optical flow estimation based on the change of the brightness of the two consequencial images are applied for velocity estimation. The novelty originates from the comprehensively investigating the dynamics of the hydrogen jet under various engine-like conditions.

Abstract: Hydrogen is a carbon-free fuel, which attracts significant attention due to its exceptional combustion properties and potential to replace conventional fossil fuels in internal combustion engine (ICE) applications. Understanding the injection and mixing dynamics of H_2 is essential to harness its advantages effectively. This study investigates the dynamics of hydrogen jets under various engine-like conditions, utilizing advanced imaging and computational techniques to provide insights critical for optimizing fuel-air mixing in direct injection (DI) engines. Two different injector configurations, a hollow cone nozzle and a modified single-hole nozzle based on piezo gasoline direct injector, were tested to explore their effects on jet behavior. To study the non-reactive H_2 jet, high-speed Z-type Schlieren imaging was employed for the visualization of density gradients within the jet under varying conditions of nozzle geometry and pressure ratio (PR, defined as injection pressure to chamber pressure). The experiment systematically analyzed the impact of these parameters on jet penetration, spread, and mixing characteristics. To estimate the velocity field of the H_2 jet, three optical flow methods, including OpticalFlow_RAFT, OpticalFlow_Farneback, and conventional OpticalFlow_PIV were applied for the velocity field estimation. The results indicated that the RAFT (Recurrent All-Pairs Field Transforms) method demonstrated the highest accuracy, particularly in identifying local velocity variations within the jet. This capability highlights the potential of RAFT as a robust tool for studying complex flow dynamics of hydrogen jets using high-speed schlieren. The novelty of this research lies integrating advanced optical diagnostics with computational analysis, which offers comprehensive examination of hydrogen jet behavior across a range of engine-relevant conditions, including nozzle geometries and pressure ratio. By this work provides valuable insights into the underlying mechanisms driving hydrogen jet dynamics. The findings contribute to the optimization of hydrogen injection strategies for next-generation ICEs, supporting the transition toward sustainable and zero-emission transportation technologies.

Key Words: Hydrogen Jet, Schlieren, Optical Flow, Velocity Field

1 INTRODUCTION

Hydrogen (H2) has gained substantial interest as a clean alternative to fossil fuels, particularly in the context of sustainable energy transitions and decarbonization goals. When produced from renewable sources, H2 combustion emits only water vapor, positioning it as a promising candidate for reducing greenhouse gas emissions in transportation, power generation, and various industrial processes. Among the strategies for H2 utilization, high-pressure injection in combustion systems stands out for its potential to enable rapid fuel-oxidizer mixing and more efficient heat release [1]. In internal combustion engines (ICEs), gas turbines, and other high-performance applications, achieving a comprehensive understanding of high-pressure H2 jets is therefore pivotal for engineering design and ensuring operational safety.

However, high-pressure H2 jets introduce several scientific and engineering challenges, including the need to characterize their transient behavior, mixing with oxidizers, ignition, and flame propagation in real-world conditions [2]. Thus, accurately estimating the velocity fields of these jets is essential to understanding and optimizing hydrogen combustion for enhanced safety, performance, and reliability. Principally, velocity fields govern the jet penetrates its environment, dictating near-field mixing and eventual combustion characteristics [3]. The dynamics of entrainment, shear-layer formation, and turbulent breakdown all hinge upon local flow speeds and directions. Moreover, velocity information is necessary to characterize the transient phenomena, such as shock waves, expansion fans, and vortex formation that arise sonic and supersonic jets during high-pressure injection [4]. These transients can significantly influence ignition and flame propagation, shaping overall efficiency and pollutant formation. Last but not the least, velocity data support the validation of computational fluid dynamics (CFD) models, which serve as predictive tools for optimizing hydrogen injection strategies in a variety of energy systems [5]. In essence, capturing the unsteady velocity fields of high-pressure H2 jets is a cornerstone for designing robust, clean, and efficient hydrogen-fueled solutions.

Historically, Particle Image Velocimetry (PIV) has been the standard experimental method for velocity field measurements in fluid mechanics [6]. By seeding the flow with tracer particles and illuminating them via pulsed lasers, PIV enables a correlation-based determination of local velocities between two or more consecutive images. Despite its successes, several constraints limit the usefulness of PIV for high-pressure H2 jets. For instance, the velocity measurement highly depends on the particle selection [7]. The unsuitable particle material or sizes could distort the flow and significantly influence the velocity accuracy. Even if robust particles are identified, achieving a uniform seeding density becomes problematic, especially under conditions where pressure fluctuates rapidly or transitions from subsonic to supersonic [8]. Additionally, high-pressure H2 jets tests generally

conducted in high-pressure constant volume chamber (CVC) to simulate the engine-like conditions. Window fouling, strong density gradients, and shock reflections can degrade image quality [9]. Ensuring that sufficient laser light is delivered and reflected within the test section to illuminate the seed particles uniformly adds another layer of complexity [10]. Furthermore, setting up a high-speed PIV system under pressurized H2 conditions requires specialized safety measures. The equipment, such as high-intensity lasers, cameras, seeding systems adds logistical constraints that can limit the range of experimental conditions explored [11]. These above limitations highlight the conventional PIV can be impractical or suboptimal for measuring velocities in high-pressure H2 flows. Researchers are thus motivated to explore alternative, seedless and more flexible methods for velocity estimation.

Schlieren imaging is an established optical technique that visualizes refractive index gradients in transparent media [12]. By collimating light through a flow and using cutoff optics (e.g., a knife edge or a focused slit) to capture slight deflections, schlieren systems produce contrast images where intensity variations correspond to density gradients. When used at high frame rates, schlieren imaging can effectively capture the evolving structure of shock waves and expansion fans in high-pressure jets. Flow features such as turbulent mixing layers, vortex and shear layers, made visible through large density gradients [13], [14]. Because schlieren imaging does not require seeding, it avoids many drawbacks of PIV. It is especially suitable for high-pressure H2 experiments, where the large density changes inherent to the jet strongly contribute to the refractive index gradients. Moreover, schlieren systems can be configured with high-speed cameras that record thousands of frames per second, capturing the fleeting dynamics of jet development.

However, schlieren imaging excels at visualizing density gradients, it does not inherently provide velocity vectors or magnitude estimates [15]. Instead, researchers interpret the evolving density features qualitatively. To bridge this gap, optical flow algorithms from computer vision can be applied to sequential schlieren images, thus enabling quantitative velocity field reconstruction [16], [17]. Optical flow in fluid dynamics contexts leverages the assumption that local intensity changes in successive frames are primarily due to fluid motion rather than illumination or background variations. Classical optical flow techniques include the Horn–Schunck (global, variational framework) [16] and Lucas–Kanade (local, correlation-based) [17] methods. The basis of the optical flow methods rely on the intensity of a point in the flow is assumed to remain constant between frames, allowing feature tracking. Neighboring velocity vectors are often encouraged to vary smoothly except at discontinuities. Adapting these principles to schlieren images can be complex, because density gradients can change in intensity due to thermodynamic effects or shock reflections [18]. Nonetheless, with careful preprocessing-such as background subtraction, contrast enhancement, and noise filtering-classical optical flow solutions can yield approximate velocity fields, especially where flow features are sharply defined and move cohesively [19]. Recent developments in deep learning have led to significant improvements in optical flow accuracy and robustness [20], [21], [22]. Neural network architectures, such as FlowNet [23], [24], PWC-Net [25], and RAFT [26], [27], are trained on large datasets of image pairs with known ground-truth motion. They learn to predict dense pixel-wise displacement fields by identifying correspondences between frames at multiple scales.

For high-pressure H2 jets, deep learning-based optical flow offers several advantages, such as 1) robust feature extraction: deep neural networks can adaptively learn feature representations that capture subtle variations in schlieren images, potentially outperforming classical algorithms in challenging flow regions or low-contrast areas [28]. 2) High-speed processing: once trained, these models can infer optical flow in near-real-time, enabling quick analysis of massive schlieren datasets generated in high-speed imaging [29]. 3) Generalization: networks exposed to a variety of synthetic or experimental flow patterns may generalize to different injection pressures, nozzle geometries, or boundary conditions, provided the training dataset is sufficiently diverse [30].

Therefore, optical flow-based velocity estimation from high-speed schlieren data holds significant promise for advancing H2 jet and combustion studies. By removing the need for seeded particles, researchers can more easily study flows at extreme pressures or temperatures where traditional PIV struggles, in particular, in the context of ultra-high-pressure H2 jets. Velocity field insights inform injector design, nozzle geometry, and injection timing. Small adjustments to these parameters can dramatically influence jet dynamics, flame stability, thermal efficiency, and pollutant formation in H2 combustion systems [31]. High-speed schlieren imaging combined with optical flow can be implemented in optical engine to observe the interplay between the H2 jet and in-cylinder flows. This integration helps guide the optimization of ignition protocols, swirl or tumble motions, and post-injection strategies. As H2-based combustion models become more sophisticated, validating

them against experimental data remains paramount [32]. High-resolution velocity fields derived from optical flow enable rigorous cross-checks of turbulence models, chemical kinetics, and boundary condition assumptions in CFD simulations.

A systematic investigation of high-speed schlieren imaging and optical flow-based velocity estimation for high-pressure H2 jets is presented, with an emphasis on how different optical flow methods perform in accurately capturing H2 jet velocities. The study begins by introducing detailed experimental analyses of H2 jets under diverse operating conditions and employing two distinct nozzle configurations. Subsequently, the theoretical foundations of optical flow in fluid dynamics are reviewed. In the results and discussion section, jet dynamics are illustrated, and three optical flow techniques are compared in estimating velocity fields at varying pressures and nozzle designs. The paper concludes with experimental validation, practical recommendations for future H2 jet research, and an outlook on incorporating these techniques into advanced H2 jet and combustion studies.

2 EXPERIMENTAL SETUP AND METHODOLOGY

In this section, the experimental setup and its components, the optical system, the test matrix, the image post-processing method, and the error analysis are described, respectively.

2.1 H2 injection system

The experimental apparatus comprises four primary circuits, as shown in Fig.1: (1) the injection line, (2) the chamber pressurizing line, (3) the exhaust line, and (4) a control system. The injection line is a three-meter hose connecting the H_2 supply cylinder to the injector; a pressure regulator and pressure sensor are integrated into this line to adjust and monitor injection pressure. Based on numerical simulations conducted with GT-Power, the three-meter hose length is sufficient to maintain a stable injection pressure during the injection phase. The second circuit, the chamber pressurizing line, runs from a nitrogen bottle rack to the constant-volume chamber and consists of a pressure regulator, a hose, and a needle valve positioned immediately upstream of the chamber. The third circuit, the exhaust line, contains (1) a spring relief valve to release pressure upon reaching the maximum chamber pressure, (2) a shut-off valve for emptying the chamber, and (3) a regulating spring valve to modulate the chamber pressure in conjunction with the gas supply. Finally, the control system employs LabVIEW software and a National Instruments driver to synchronize the injector with a high-speed camera (Phantom V2012), while also collecting real-time chamber pressure and temperature measurements through dedicated sensors.

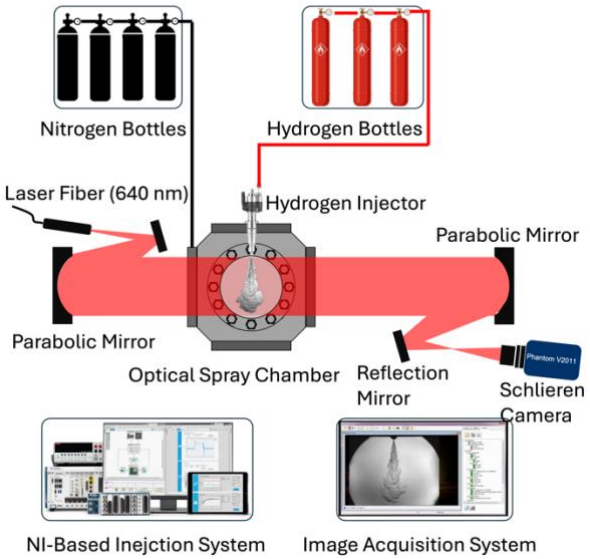

Fig. 1 Experimental setup for the high-pressure H_2 jet using schlieren imaging

Fig. 2 depicts the hollow-cone outwardly opening injector utilized for high-pressure H2 jet studies. This injector originally designed as a commercially available gasoline direct injection (GDI) injector by Siemens VDO Automotive, it operates at rail pressures of up to 200 bar. The cross-sectional view highlights the injector's advanced design, featuring a needle directly actuated by a piezoelectric stack. This stack is controlled by a National Instruments control unit, which precisely adjusts the voltage and current profiles, enabling fine-tuned regulation of the needle lift. This precise control allows for accurate manipulation of the injector's opening and closing speeds, ensuring optimal injection performance.

To explore the influence of nozzle configuration on H2 jet dynamics, the injector was modified from its original hollow-cone design to a single-hole nozzle. This modification facilitates fundamental studies of H_2 jet behavior, providing deeper insights into the role of nozzle geometry in governing jet characteristics under high-pressure conditions.

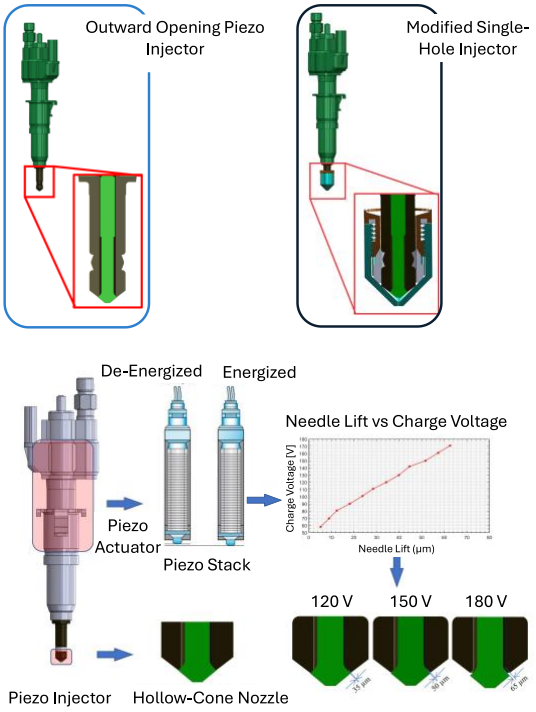

Fig.2 Schematic of piezeo injector used for the high-pressure H2 jets

2.2 High-speed schlieren imaging

In this study, a high-speed Z-type Schlieren imaging technique is employed to visualize the H_2 jets, providing detailed insights into flow dynamics. The Schlieren system, essentially a shadowgraph enhanced with a schlieren cutoff (e.g., a knife edge or iris), operates on the principle that light rays bend when encountering fluid density gradients. In the Z-type Schlieren configuration, traditional lenses are replaced with parabolic concave mirrors due to two significant advantages. First, mirrors are free from chromatic aberrations, unlike lenses. Second, while achromatic lenses can minimize chromatic aberrations, they are prohibitively expensive, especially for large free aperture diameters [32].

Figure 2 illustrates a schematic of the high-speed Z-type Schlieren system. In this setup, a collimated light beam from a high-power monochromatic laser (Cavitar Smart) spotlight, reflected by a mirror, illuminates the jet. As the light passes through the jet, density gradients cause refraction. A second parabolic mirror focuses the refracted light onto the lens of the high-speed camera, positioned behind an iris. The iris partially obstructs refracted light beams, creating high-contrast Schlieren images. Due to the high chamber pressures and associated safety considerations, the injector is mounted on the top center of the chamber, with visualization conducted through lateral quartz windows. Although the inclusion of quartz windows in the optical path can degrade image quality [32], this issue is effectively mitigated using background subtraction during image post-processing.

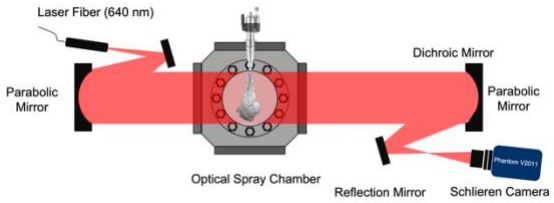

Fig.3 Schematic of the z-type schlieren imaging system

Table 1 details the components of the optical system, including specifications of the Schlieren setup. This configuration ensures reliable and high-quality imaging of the dynamic hydrogen jet under engine-relevant conditions.

Table 1. Optical system components.

Component	Feature
Electrical power of the LED	High-speed schlieren with wavelength of 640 nm
Diameter of aperture's slit	3 mm
Focal length of first mirror	609,6 mm
Focal length of second mirror	762 mm
Percentage of the knife-edge cut-off	Approximately 60%
Exposure time of the camera	10 µs
Frame rate	34,000
Resolution	768 × 768

2.3 High-speed schlieren imaging

Fig.4 demonstrates the post-processing workflow for Schlieren images of H_2 jets using two different injectors: an outward-opening piezo injector and a modified single-hole injector. Starting with the raw Schlieren images capturing the density gradients in the jet, the region of interest is isolated through image cropping. A 2D convolution is then applied to enhance the edges of the jets and highlight key features within the flow. This is followed by binarization, where the jet is segmented from the background by assigning distinct intensity values to the jet and non-jet regions. Finally, boundary detection is performed to outline the jet structure, with the detected contours superimposed on the original image for clear visualization. This systematic process enables precise analysis of jet dynamics, such as shape, penetration, and mixing behavior, while facilitating a direct comparison between the effects of different nozzle geometries.

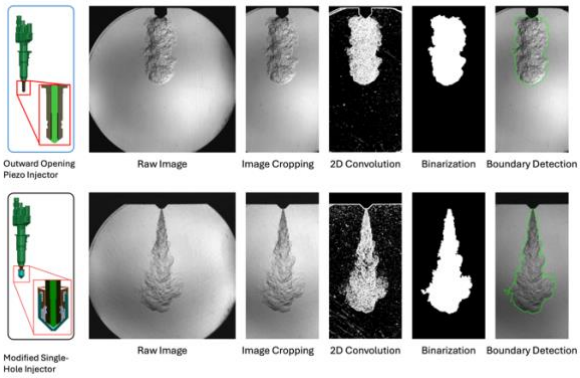

Fig.4 Workflow of the image post-processing for hollow-cone and single-hole injectors

2.4 Optical flow method

The domain of optical flow estimation has advanced considerably since its inception in the 1950s [21]. A fundamental principle in this field is the brightness constancy constraint, which posits that the intensity of a pixel remains unchanged as it moves within successive frames. Formally, this principle is expressed as:

$$\frac{\partial I}{\partial t} + u\frac{\partial I}{\partial x} + v\frac{\partial I}{\partial y} = 0 \quad (1)$$

where I represents the image intensity, u and v are the horizontal and vertical components of the optical flow vector, and $\frac{\partial I}{\partial t}$, $\frac{\partial I}{\partial x}$, and $\frac{\partial I}{\partial y}$ are the temporal and spatial derivatives of I.

However, the brightness constancy constraint inherently leads to the aperture problem, as illustrated in Fig.5. The upper row shows the actual movement of the purple rectangle, while the lower row depicts perceived movement of the purple rectangle on the smaller area (green). It can be seen that only the horizontal component of the motion is evident. This issue arises from the inability to uniquely determine the motion of object based on local information observed through a limited spatial region (the "aperture"). Mathematically, solving for the motion components u and v using only Eq. (1) results in an underdetermined system, as it provides a single equation with two unknowns. To overcome this limitation and establish a well-posed framework, it is necessary to incorporate additional constraints or regularization assumptions that leverage spatial or temporal coherence in the motion field.

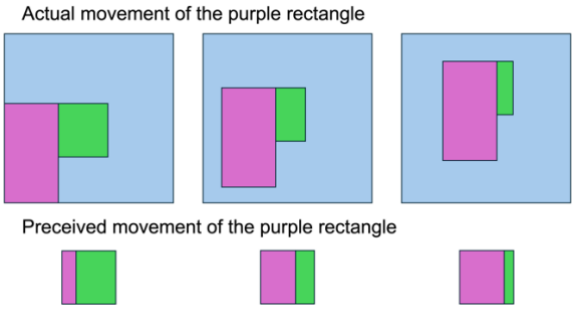

Fig.5 Depiction of the aperture problem of the conventional optical flow method [21].

To address these challenges, two classical variational frameworks are commonly employed for estimating dense optical flow from sequential frames. The first is the global Horn-Schunck (HS) method [16], which imposes a global smoothness constraint across the entire image. The second is the local Lucas-Kanade (LK) method [17], which instead relies on local constancy assumptions to infer motion.

The HS method tackles the aperture problem and mitigates flow distortions by introducing a global smoothness constraint, which ensures gradual flow variations across adjacent pixels. This approach formulates optical flow estimation as the minimization of a global energy functional, expressed as:

$$E = \iint \left[\left(I_x u + I_y v + I_t\right)^2 + \alpha^2 (\|\nabla u\|^2 + \|\nabla v\|^2) \right] dxdy \quad (2)$$

where I_x, I_y , I_t and are gradients of the image intensity along the x, y, and time dimensions, respectively, $u(x,y)$ and $v(x,y)$form the optical flow vector at position (x,y), α is a regularization constant that controls the balance between data fidelity and smoothness in the estimated flow, and ∇u and ∇v denote the spatial gradients of the optical flow components.

$$I_x(p) \cdot V_x + I_y(p) \cdot V_y = I_t(p) \quad (3)$$

By aggregating data from nearby pixels $(q_1, q_2, \cdots, q_n)$ the LK method sets up a system of linear equations $Av = b$:

$$A = \begin{bmatrix} I_x(q_1) & I_y(q_1) \\ I_x(q_2) & I_y(q_2) \\ \vdots & \vdots \\ I_x(q_n) & I_y(q_n) \end{bmatrix}, v = \begin{bmatrix} V_x \\ V_y \end{bmatrix}, b = \begin{bmatrix} -I_t(q_1) \\ -I_t(q_2) \\ \vdots \\ -I_t(q_n) \end{bmatrix} \quad (4)$$

As this system is generally overdetermined, the LK method uses the least squares principle, solving for v as:

$$v = (A^T A)^{-1} A^T b \quad (5)$$

Despite the foundational progress achieved by the HS and LK methods, handling intricate flow scenarios remains an active area of research, prompting the development of more sophisticated optical flow estimation techniques. For instance, high-order pyramid smoothness constraints [33] have been proposed to preserve motion boundaries and improve performance in complex scenes. Methods like DeepFlow [34] and EpicFlow [35] combine traditional variational frameworks with feature-matching approaches to track motion between consecutive frames, effectively addressing large displacements [36]. The emergence of deep learning further revolutionized the field, beginning with FlowNet [23], which introduced FlowNet-S and FlowNet-C architectures based on the encoder–decoder U-Net [37]. FlowNet 2.0 [24] subsequently built on these designs by stacking multiple FlowNet modules to achieve substantially improved accuracy[38]. Meanwhile, SPyNet [39] offered a compact, coarse-to-fine approach that trades off some accuracy to handle large motions. More recently, PWC-Net [25] integrated feature extraction, cost volume, and stereo matching concepts into a modified spatial pyramid network, whereas RAFT [26] introduced recurrent all-pairs field transforms and a recurrent update operator, offering a novel perspective on optical flow estimation that diverges from traditional spatial pyramidal strategies.

Among all above optical flow methods, RAFT offers an estimation of Dense Optical Flow assigns each pixel a 2D flow vector describing the horizontal and vertical displacement over a time interval based on a comprehensive all-pairs correlation volume and a recurrent refinement mechanism. First, RAFT extracts features from both images in a pair, then constructs a multi-scale correlation volume that encodes similarity scores between every pixel in the first image and every pixel in the second. Unlike earlier optical flow methods that rely on explicit warping or coarse-to-fine pyramids, correlation volume of RAFT remains in a consistent feature space, allowing local and global cues to be captured without repeated spatial downsampling. Once the correlation volume is established, RAFT employs a recurrent unit to iteratively refine the flow field. At each iteration, the model uses the correlation volume to query motion information and update the flow estimate in a pixel-wise manner. This iterative process enables the network to correct errors from previous iterations by focusing on local details and larger-scale context, while maintaining a constant resolution for all flow updates. As a result, RAFT typically achieves both high accuracy and robustness, outperforming many prior optical flow models on standard benchmarks.

In this study, three distinct optical flow methods were selected for velocity field estimation- OpticalFlow_RAFT (a deep learning-based approach), OpticalFlow_Farneback (a classical optical flow method), and OpticalFlow_PIV (an image-based adaptation of conventional Particle Image Velocimetry). This combination enables a systematic comparison of modern deep learning, traditional variational, and PIV-derived techniques under the same experimental conditions.

3 RESULTS AND DISCUSSIONS

This section presents the experimental results for H_2 jets under varying conditions and utilizing two distinct nozzle configurations. First, it highlights the differences in overall jet structure between hollow-cone and single-hole nozzles. Next, it examines how pressure ratio and nozzle geometry influence jet penetration, cross-sectional area, volume, and tip velocity. Finally, the velocity field estimations obtained from OpticalFlow_RAFT, OpticalFlow_Farneback, and OpticalFlow_PIV are compared to evaluate their relative performance.

3.1 Jet structure

Prior to the quantitative analysis of the H2 jet, the macroscopic jet structure over consecutive time intervals is compared with various conditions and nozzle configurations.

Fig. 6 and 7 illustrate H_2 jets injected from hollow-cone and single-hole nozzles at a pressure ratio of 20 and10 (i.e., Pinj=100 bar, Pch=5bar) with a needle lift of 25 µm. For the hollow-cone nozzle, the jet exhibits a distinct outwardly expanding structure. At the initial stages (0.32 ms ASOI), the jet shows a small, rounded plume near the injector tip, indicating the initial penetration phase. As time progresses, the jet expands radially outward, forming a broader conical shape (visible at 0.62 ms and beyond). By 1.5 ms ASOI, the hollow-cone jet demonstrates significant radial spread, with a relatively uniform density distribution across the plume, reflecting effective dispersion but limited axial penetration. In contrast, the single-hole nozzle produces a highly collimated and elongated jet. At 0.32 ms ASOI, the jet appears narrow and concentrated, with clear axial penetration. Over time (0.62 ms to 1.5 ms ASOI), the single-hole jet maintains its streamlined shape, extending further axially into the chamber. The boundary of the jet shows less radial expansion compared to the hollow-cone nozzle, emphasizing its focused delivery and higher penetration depth.

Overall, the hollow-cone nozzle promotes broader radial dispersion, potentially enhancing fuel-air mixing over a larger volume, while the single-hole nozzle achieves greater axial penetration, suitable

for targeted injection strategies. These differences highlight the influence of nozzle geometry on jet dynamics, with each design tailored for specific mixing and combustion requirements in hydrogen-fueled engines.

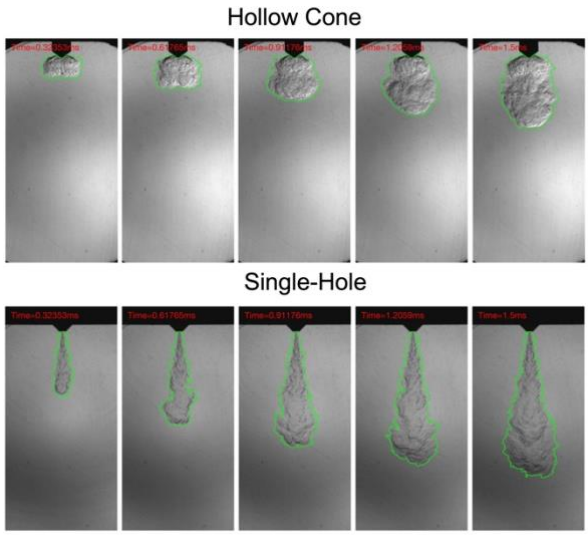

Fig. 6 The H_2 jets injected from hollow-cone and single-hole nozzles at a pressure ratio of 20 (i.e., P_{inj}=100 bar, P_{ch}=5bar) and a needle lift of 25 µm

Fig.7 shows the jet evolution under the pressure ratio of 10 with increasing the chamber pressure from 5 bar to 10 bar. The jet expansion is noticeably more restricted compared to PR = 20, with slower radial growth and a smaller cone diameter at each time step. The reduced momentum results in lower penetration and dispersion, indicating that the H_2 jet is less energetic and more localized.

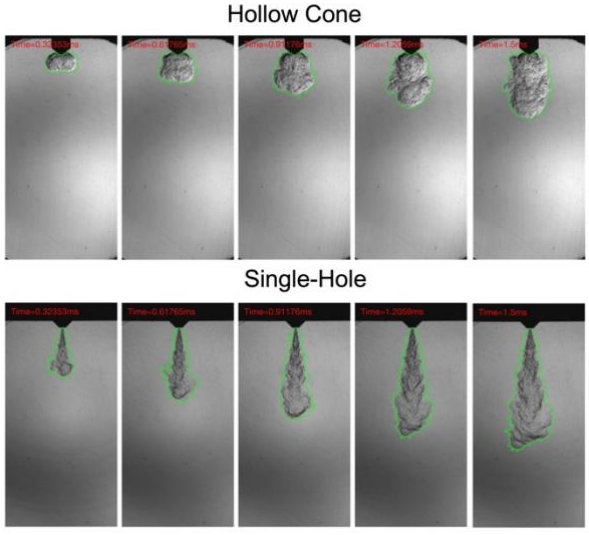

Fig. 7 The H_2 jets injected from hollow-cone and single-hole nozzles at a pressure ratio of 10 (i.e., P_{inj}=100 bar, P_{ch}=10bar) and a needle lift of 25 µm

To further estimate the jet structure from the hollow-cone and single-hole nozzles, the jet-to-jet variations are compared with 10 repetitions. Fig. 8 and 9 demonstrate the jet-to-jet variation and averaged jets from hollow-cone and single-hole nozzles at a pressure ratio of 20 and10 (i.e., Pinj=100 bar, Pch=5bar) with a needle lift of 25 µm. The results indicate that both nozzles show very low jet-to-jet variation in the jet structure with more 90% of area of the jet over 10 injections, which highlight the relability for the furture investigations. While the single-hole nozzle shows greater jet-to-jet variation, particularly in the radial expansion of the jet boundaries. This could be due to the complex dynamics of the H2 and air entrainments with higher jet tip velocity, which leads to fluctuations in the distribution of the jet. The averaged jet structure of the hollow-cone nozzle highlights its broader dispersion, which promotes fuel-air mixing over a larger volume, while averaged jet structure of the single-hole nozzle emphasizes its focused and highly directional penetration, suitable for applications requiring precise injection.

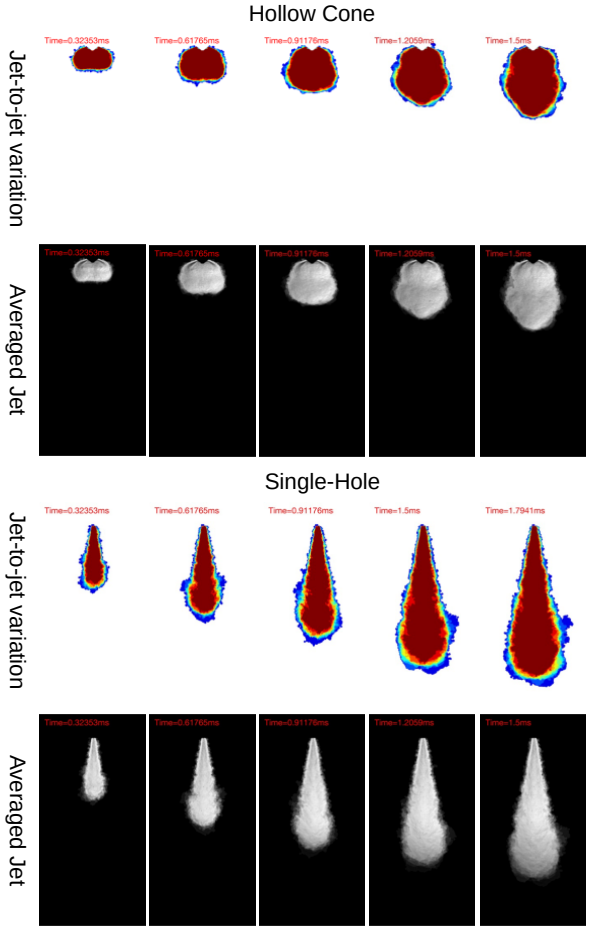

Fig. 8 The jet-to-jet variation and averaged jets from hollow-cone and single-hole nozzles at a

pressure ratio of 20 (i.e., P_{inj}=100 bar, P_{ch}=5 bar) and a needle lift of 25 µm

Fig.9 demonstrates the jet-to-jet variation and averaged jets from hollow-cone and single-hole nozzles at a pressure ratio of 10 (i.e., P_{inj}=100 bar, P_{ch}=10bar) and a needle lift of 25 µm. Compared to the higher pressure ratio both nozzles, the jets at lower pressure ratio exhibit reduced axial and radial dispersion due to the lower injection momentum. The outward expansion is less pronounced, resulting in a smaller jet structure. Jet-to-jet variations are limited because the lower pressure ratio generates a more stable injection with reduced turbulence. The averaged jet structure is compact, with slower growth over time. The lower energy limits the ability of the H_2 to overcome chamber resistance, leading to less effective mixing.

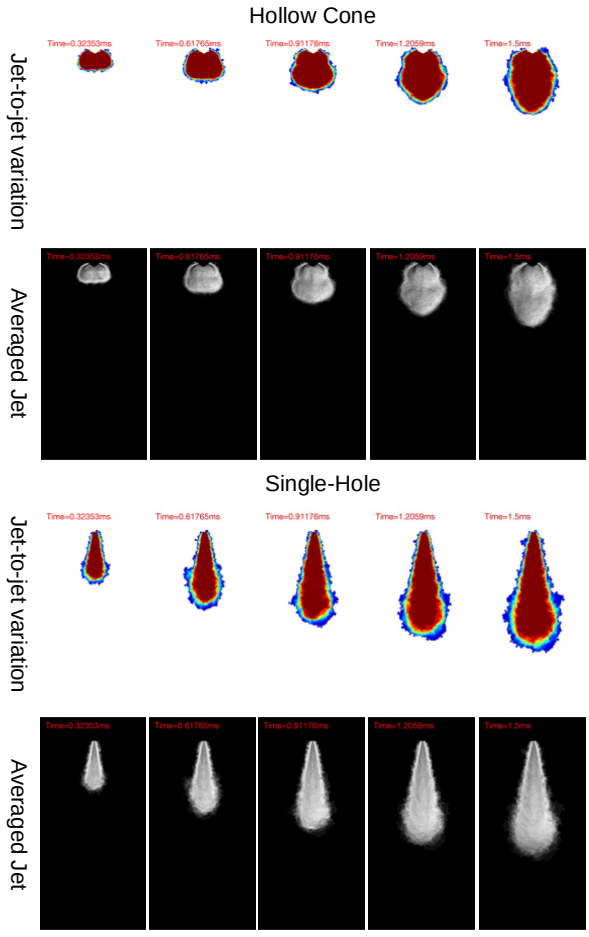

Fig. 9 The jet-to-jet variation and averaged jets from hollow-cone and single-hole nozzles at a pressure ratio of 10 (i.e., P_{inj}=100 bar, P_{ch}=10bar) and a needle lift of 25 µm

3.2 Hydrogen jet evolution

Fig. 10 shows the quantitative jet evolution based on the image post-processing. The findings reveal distinct characteristics of H2 jets under different injection pressure ratios (Pr) and nozzle configurations. Higher pressure ratios (Pr = 20) significantly enhance both penetration and mixing efficiency, with the single-hole nozzle demonstrating the fastest jet penetration and highest velocity due to its focused and streamlined design, making it suitable for targeted fuel delivery. Conversely, the hollow-cone nozzle exhibits shorter jet penetrations, areas, jet volumes, even though facilitating better radial dispersion and mixing. However, with increased chamber pressure (higher chamber density), jet expansion is suppressed, reducing penetration and radial spread for both nozzles. Lower Pr results in slower jets with reduced penetration and mixing potential, while higher chamber densities enhance stability but further limit jet growth. These findings emphasize the trade-offs between mixing efficiency and penetration, highlighting the influence of nozzle geometry and operating conditions on H2 jet dynamics.

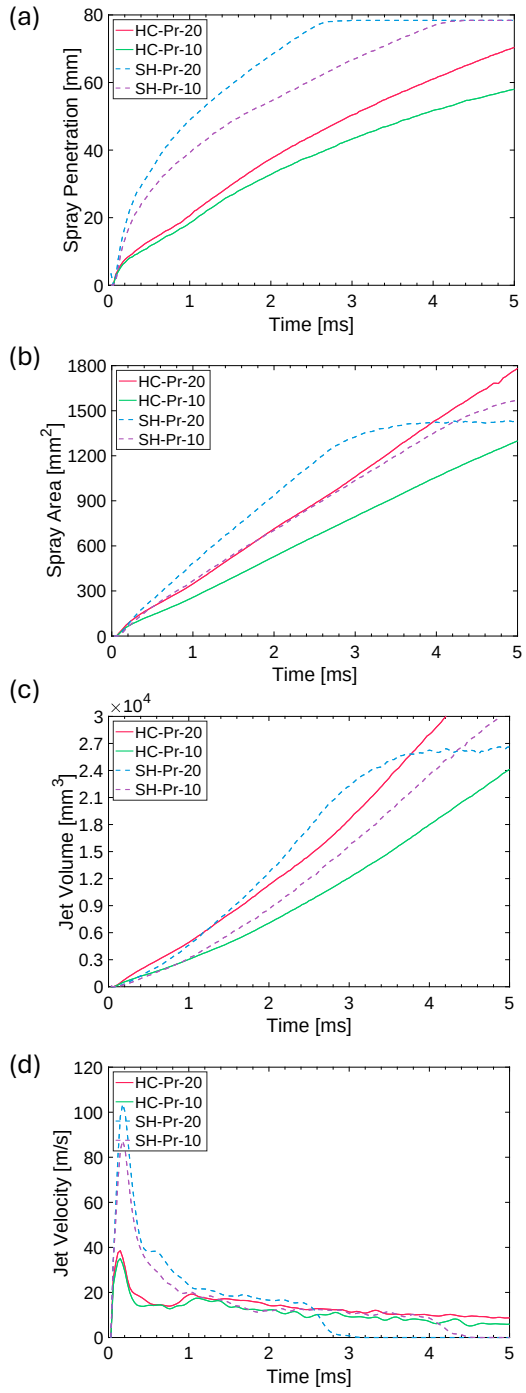

Fig. 10 H_2 jet evolution under Pr=20 and Pr=10 with hollow-cone (HC) and single-hole(SH) nozzles

3.3 Velocity estimation of hydrogen jet

Fig. 11 compares the velocity fields of the H_2 jet estimated using three optical flow methods: (a) OpticalFlow_RAFT, (b) OpticalFlow_Farneback, and (c) OpticalFlow_PIV. Fig.11(a) indicates that RAFT provides highly detailed and dense vector fields, capturing small-scale local velocity variations within the jet. The resolution of the vectors is consistent, especially in regions of high turbulence near the jet boundaries.The vectors are well-aligned with the flow direction, indicating a precise representation of jet dynamics. RAFT captures a wide range of velocity magnitudes with clear differentiation between high-velocity core regions and low-velocity jet peripheries. Velocity peaks are observed near the injection point, gradually decreasing as the jet disperses. The method effectively highlights localized high-velocity regions.

Fig.11(b) shows that Farneback generates a relatively sparse vector field compared to RAFT, with less detail in turbulent regions. The vectors are smoother, but some directional inconsistencies appear in high-gradient regions. The method captures the general flow direction but struggles with finer details, particularly in regions of rapid velocity change. Meanwhile, Farneback provides a smoother magnitude distribution but lacks the ability to differentiate high-velocity cores from low-velocity regions effectively. Velocity magnitudes are generally underestimated compared to RAFT, leading to less precise characterization of jet dynamics.

The conventional OpticalFlow_PIV method is presented in Fig.11(c), which indicates that this method produces a moderate-density vector field, with clear and consistent alignment along the jet axis. However, the vectors are too mess and need to be further smoothen manually. The method performs well in capturing large-scale jet dynamics but loses detail in regions of complex turbulence. Additionally, the OpticalFlow_PIV shows clear velocity magnitude gradients, with a sharp distinction between the high-velocity core and the surrounding low-velocity regions.

Among the methods, RAFT stands out for its ability to resolve fine-scale details and accurately capture velocity magnitude distributions, making it the most reliable choice for high-resolution hydrogen jet analysis. OpticalFlow_PIV provides a good balance between accuracy and computational efficiency for large-scale studies, while Farneback is limited to capturing general trends with lower precision. These findings highlight the trade-offs between

resolution, accuracy, and computational demands across the optical flow methods.

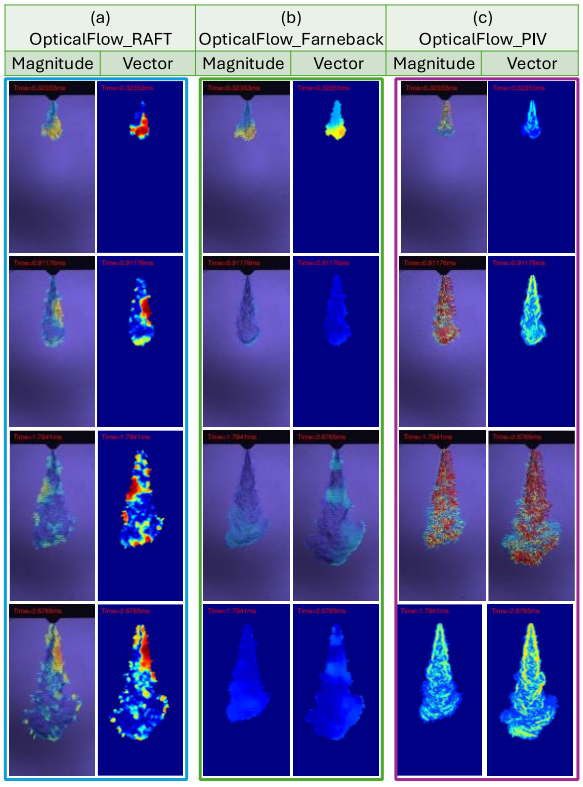

Fig. 11 The comparison of three optical flow methods on the H_2 jet velocity estimation with a single-hole nozzle and Pr=20, (a) OpticalFlow_RAFT, (b) OpticalFlow_Farneback and (c) OpticalFlow_PIV

Fig. 12 and Fig. 13 demonstrates the velocity field of the H_2 jet from hollow-cone and single-hole nozzles at a pressure ratio of 20 (i.e., P_{inj}=100 bar, P_{ch}=10bar) and 10 (i.e., P_{inj}=100 bar, P_{ch}=10bar). The velocity field comparison between the hollow-cone and single-hole nozzles highlights their distinct flow characteristics. The hollow-cone nozzle exhibits a broad radial dispersion, with velocity vectors distributed outward in a symmetrical cone-like pattern. Velocity magnitudes are relatively low due to the energy spreading across a wider area, resulting in a slower, less focused jet. In contrast, the single-hole nozzle produces a more collimated jet with concentrated velocity vectors aligned along the jet axis, indicating higher axial penetration and greater velocity magnitudes near the core. Regarding to the velocity estimation, the velocity field estimation on the hollow-cone jets shows challenges in accurately resolving fine-scale details due to the broad radial dispersion, where velocity vectors are widely distributed. This dispersion leads to lower velocity magnitudes and potential underestimation of localized flow dynamics near the edges of the spray. However, for the single-hole nozzle, due to more collimated jet, the velocity field estimation captures the high axial velocities with better precision in the downstream of the jet, particularly along the jet core. But in the near-nozzle and center-line region, due to the denser optics and less contrast, the flow velocity could be under predicted. Overall, the single-hole nozzle's concentrated flow provides a more straightforward and accurate estimation of velocity fields, while the hollow-cone nozzle introduces complexity due to its dispersed and multi-directional flow, potentially affecting the resolution of smaller velocity gradients and turbulence.

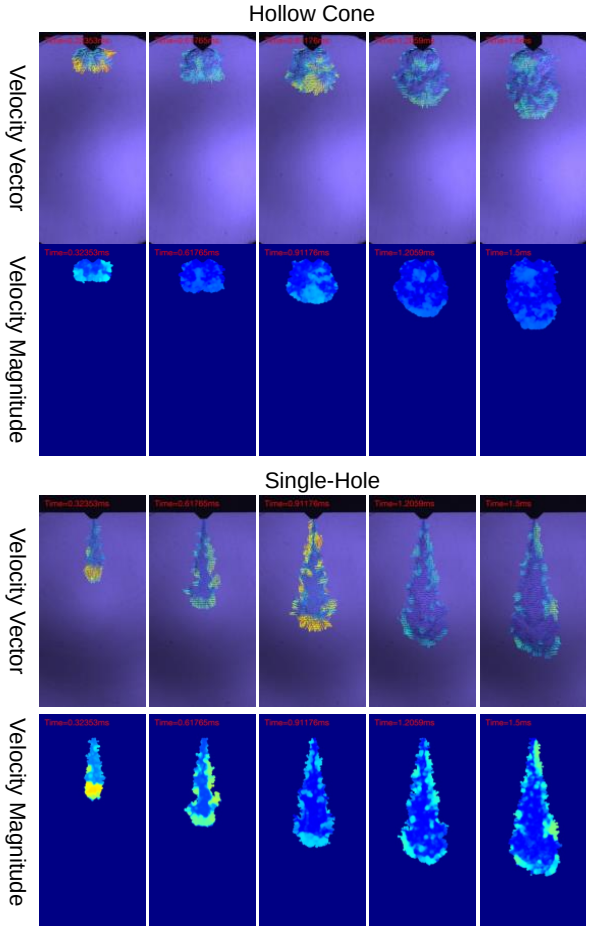

Fig. 12 The velocity field estimation of the H_2 jets from hollow-cone and single-hole nozzles at a pressure ratio of 20 (i.e., P_{inj}=100 bar, P_{ch}=5 bar)

Fig. 13 demonstrates the comparison between high (Pr = 20) and low (Pr = 10) pressure ratios reveals significant differences in jet dynamics for both hollow-cone and single-hole nozzles. At a high pressure ratio, the hollow-cone nozzle exhibits stronger radial dispersion with higher velocity magnitudes and a well-defined conical structure, while the single-hole nozzle demonstrates deeper axial penetration with concentrated high-velocity

vectors along the jet axis. In contrast, at a low pressure ratio, the hollow-cone jet becomes more compact with reduced radial spread and lower velocities, while the single-hole jet shows diminished penetration and weaker velocity magnitudes. The higher pressure ratio enhances energy and momentum transfer, resulting in more dynamic and energetic jets with better velocity field resolution, whereas the lower pressure ratio produces weaker jets with limited dispersion and penetration, reducing their overall effectiveness for mixing and injection applications.

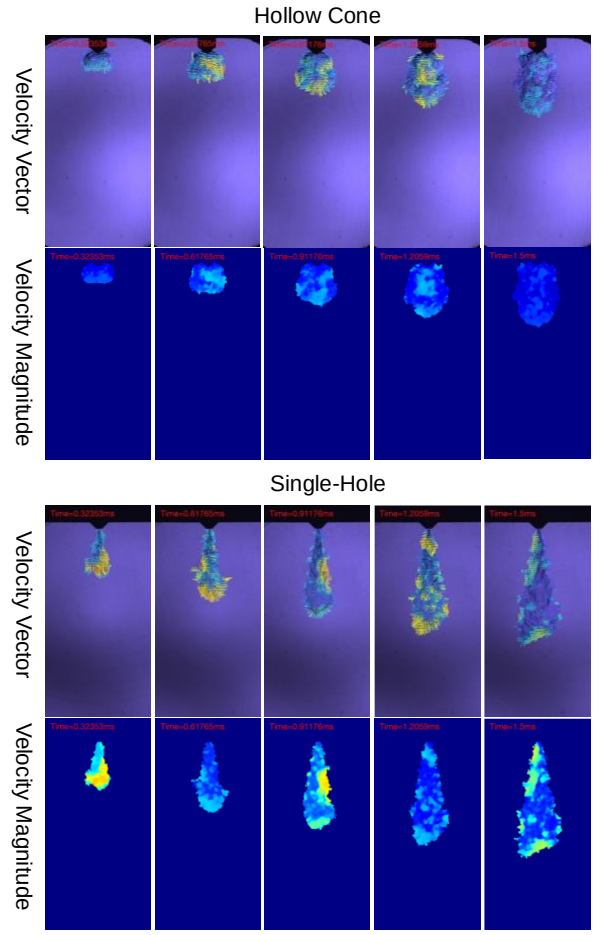

Fig. 13 The velocity field estimation of the H_2 jets from hollow-cone and single-hole nozzles at a pressure ratio of 10 (i.e., P_{inj}=100 bar, P_{ch}=10 bar)

4 CONCLUSION

This study provides a detailed investigation of high-pressure H_2 jets, focusing on the velocity field dynamics of hollow-cone and single-hole nozzles under varying pressure ratios (Pr = 20 and Pr = 10). The key findings are summarized as follows:

(1) The hollow-cone nozzle exhibits significant radial dispersion, making it ideal for enhancing fuel-air mixing, whereas the single-hole nozzle achieves superior axial penetration with a focused and collimated jet structure. Higher pressure ratios amplify jet energy, resulting in enhanced penetration, dispersion, and better-resolved velocity fields for both nozzles, while lower pressure ratios lead to weaker jets with reduced penetration and mixing efficiency.

(2) To estimate the velocity fields of H_2 jets, three optical flow methods, including OpticalFlow_RAFT, OpticalFlow_Farneback, and OpticalFlow_PIV are compared. The results demonstrate that OpticalFlow_RAFT provides the most accurate velocity estimations, effectively capturing fine-scale turbulence and high-resolution velocity gradients, making it ideal for detailed jet dynamics analysis. OpticalFlow_PIV offers a balance between accuracy and computational efficiency, capturing large-scale velocity trends effectively but lacking the resolution for fine turbulence details. In contrast, OpticalFlow_Farneback is computationally efficient but underestimates velocity magnitudes and struggles to resolve complex velocity fields, making it less suitable for precise jet characterization.

(3) The study identifies challenges in velocity estimation for hollow-cone nozzles, where broad radial dispersion complicates the resolution of fine-scale turbulence. In comparison, the single-hole nozzle with concentrated flow structure allows for higher accuracy in velocity estimation, particularly in downstream regions. However, near-nozzle regions for both nozzles may show reduced precision due to optical limitations.

(4) According to the jet behavior and velocity estimation using schlieren imaing combined with advanced optical flow methods, it provides critical insights for optimizing H_2 injection strategies. These insights help balance mixing efficiency and precise delivery for H_2-fueled, zero-emission combustion technologies.

5 FUTURE WORK

However, due to time constraints, the optical flow methods used in this study have not been rigorously validated against ground truth data, such as particle image velocimetry (PIV) measurements or computational fluid dynamics (CFD) simulations. Future work will focus on a systematic validation of these optical flow methods under controlled conditions to quantify their performance, particularly in resolving fine-scale turbulence and

velocity gradients. Additionally, exploring advanced hybrid methods or incorporating machine learning-based velocity estimation techniques may improve the accuracy and efficiency of velocity field analysis.

6 ACKNOWLEDGMENTS

This work was supported by the Ultra-H_2 project funded by Research Council of Finland (Grant No. 363936) and HENNES (Hydrogen combustion simulation tools and experiments) project funded by Business Finland (Grant No. 211914) are acknowledged. Our sincere gratitude extends to MSc. Olli Ranta and MSc. Otto Blomstedt for technical assistance.

7 REFERENCES AND BIBLIOGRAPHY

1. Delbari, H., S. Munshi, and G. McTaggart-Cowan, Characterizing injection and ignition of hydrogen and hydrogen-methane blend fuels in a static combustion chamber. Fuel, 2025. 381: p. 133562.

2. Bae, G., J. Lee, and S. Moon, Transient development and structure of supersonic gas jets from narrow-cone-angle pintle-type hydrogen injector. Fuel, 2025. 384: p. 134072.

3. Coratella, C., A. Tinchon, R. Oung, L. Doradoux, G. Dober, C. Hespel, and F. Foucher, Experimental characterization of a hydrogen hollow cone jet at under-expanded conditions via schlieren technique. International Journal of Hydrogen Energy, 2024. 72: p. 730-743.

4. Lu, S., J. Fan, and K. Luo, High-fidelity resolution of the characteristic structures of a supersonic hydrogen jet flame with heated co-flow air. International Journal of Hydrogen Energy, 2012. 37(4): p. 3528-3539.

5. Li, X., K. Wu, W. Yao, and X. Fan, A comparative study of highly underexpanded nitrogen and hydrogen jets using large eddy simulation. International Journal of Hydrogen Energy, 2016. 41(9): p. 5151-5161.

6. Chen, F. and H. Liu, Particle image velocimetry for combustion measurements: Applications and developments. Chinese Journal of Aeronautics, 2018. 31(7): p. 1407-1427.

7. Wereley, S.T. and C.D. Meinhart, Recent Advances in Micro-Particle Image Velocimetry. Annual Review of Fluid Mechanics, 2010. 42(Volume 42, 2010): p. 557-576.

8. Westerweel, J., G.E. Elsinga, and R.J. Adrian, Particle Image Velocimetry for Complex and Turbulent Flows. Annual Review of Fluid Mechanics, 2013. 45(Volume 45, 2013): p. 409-436.

9. Melling, A., Tracer particles and seeding for particle image velocimetry. Measurement Science and Technology, 1997. 8(12): p. 1406.

10. Willert, C.E., High-speed particle image velocimetry for the efficient measurement of turbulence statistics. Experiments in Fluids, 2015. 56(1): p. 17.

11. Xing, F., D. Wang, H. Tan, K. Wang, B. Lin, and D. Zhang, High-resolution light-field particle imaging velocimetry with color-and-depth encoded illumination. Optics and Lasers in Engineering, 2024. 173: p. 107921.

12. Lai, B., H. Li, S. Wang, Z.-Q.J. Xu, J. Song, Y. Liu, and X. Wen, Analysis of high subsonic sweeping jet external flow characteristics and velocity using schlieren visualization and schlieren image velocimetry method. Experimental Thermal and Fluid Science, 2025. 163: p. 111397.

13. Vishnoi, N., A. Saurabh, and L. Kabiraj, Schlieren Image Velocimetry and Modal Decomposition Study of Preheated Isothermal Flow From a Generic Multi-Swirl Burner. Journal of Engineering for Gas Turbines and Power, 2024. 147(1).

14. Li, G., H. Sun, Q. Tang, H. Zhen, H. Wang, H. Liu, and M. Yao, Fundamental insights on turbulence characterization, vortex motion and ignition mechanism of sub/supersonic turbulent jet flames. Applied Thermal Engineering, 2024. 248: p. 123274.

15. Chen, M., Z. Zhao, X. Wang, Z. Wang, F. Li, J. Zhu, M. Sun, and B. Zhou, Wavelet optical flow velocimetry of a scramjet combustor using high-speed frame-straddling focusing schlieren images. Combustion and Flame, 2024. 269: p. 113705.

16. Horn, B.K.P. and B.G. Schunck, Determining optical flow. Artificial Intelligence, 1981. 17(1): p. 185-203.

17. Lucas, B., D and T. Kanade, An Iterative Image Registration Technique with an Application to Stereo Vision, in IJCAI'81: 7th international joint conference on Artificial intelligence. 1981: Vancouver, Canada. p. 674-679.

18. Chen, M., Z. Zhao, Y. Hou, J. Zhu, M. Sun, and B. Zhou, Evaluation of seedless wavelet-based

optical flow velocimetry for schlieren images. Physics of Fluids, 2024. 36(7).

19. Liu, T. and D.M. Salazar, Two-dimensional vector field topology and scalar fields in viscous flows: Reconstruction methods. Physics of Fluids, 2024. 36(7).

20. Wang, Y., W. Wang, Y. Li, J. Guo, Y. Xu, J. Ma, Y. Ling, Y. Fu, and Y. Jia, Research on traditional and deep learning strategies based on optical flow estimation - a review. Journal of King Saud University - Computer and Information Sciences, 2024. 36(4): p. 102029.

21. Alfarano, A., L. Maiano, L. Papa, and I. Amerini, Estimating optical flow: A comprehensive review of the state of the art. Computer Vision and Image Understanding, 2024. 249: p. 104160.

22. Adil, O., M.A. Mahraz, J. Riffi, and H. Tairi. Advancements in Deep Learning-Based Optical Flow Estimation: A Comprehensive Review of Models and Techniques. in 2024 Sixth International Conference on Intelligent Computing in Data Sciences (ICDS). 2024.

23. Dosovitskiy, A.a.F., Philipp and Ilg, Eddy and Hausser, Philip and Hazirbas, Caner and Golkov, Vladimir and van der Smagt, Patrick and Cremers, Daniel and Brox, Thomas, FlowNet: Learning Optical Flow With Convolutional Networks, in Proceedings of the IEEE International Conference on Computer Vision (ICCV). 2015.

24. Ilg, E.a.M., Nikolaus and Saikia, Tonmoy and Keuper, Margret and Dosovitskiy, Alexey and Brox, Thomas, FlowNet 2.0: Evolution of Optical Flow Estimation With Deep Networks, in Proceedings of the IEEE Conference on Computer Vision and Pattern Recognition (CVPR). 2017.

25. Sun, D.a.Y., Xiaodong and Liu, Ming-Yu and Kautz, Jan},, PWC-Net: CNNs for Optical Flow Using Pyramid, Warping, and Cost Volume, in Proceedings of the IEEE Conference on Computer Vision and Pattern Recognition (CVPR). 2018.

26. Teed, Z. and J. Deng. RAFT: Recurrent All-Pairs Field Transforms for Optical Flow. in Computer Vision – ECCV 2020. 2020. Cham: Springer International Publishing.

27. Lagemann, C., K. Lagemann, S. Mukherjee, and W. Schröder, Deep recurrent optical flow learning for particle image velocimetry data. Nature Machine Intelligence, 2021. 3(7): p. 641-651.

28. Liu, Z., X. Wu, Z. Liu, J. Zhang, H. Yue, and W. Chen. CrossTR-Raft :Dense optical flow estimation based on cross attention mechanisms. in 2024 IEEE 19th Conference on Industrial Electronics and Applications (ICIEA). 2024.

29. Shiba, S., Y. Klose, Y. Aoki, and G. Gallego, Secrets of Event-Based Optical Flow, Depth and Ego-Motion Estimation by Contrast Maximization. IEEE Transactions on Pattern Analysis and Machine Intelligence, 2024. 46(12): p. 7742-7759.

30. Akhavan-Safaei, A. and M. Zayernouri DEEP LEARNING MODELING FOR SUBGRID-SCALE FLUXES IN THE LES OF SCALAR TURBULENCE AND TRANSFER LEARNING TO OTHER TRANSPORT REGIMES. 2024. 5(1): p. 1-23.

31. Wu, Z., Q. Cheng, X. Gu, Z. Wang, L. Lu, X. Pan, M. Hua, J. Xiao, and J. Jiang, Experimental investigation on the development characteristics of high-pressure hydrogen jet flame under different ignition conditions. International Journal of Hydrogen Energy, 2024. 79: p. 791-801.

32. Yeganeh, M., M.S. Akram, Q. Cheng, S. Karimkashi, O. Kaario, and M. Larmi, Experimental study of hydrogen jet dynamics: Investigating free momentum and impingement phenomena. International Journal of Hydrogen Energy, 2024. 68: p. 1423-1437.

33. Brox, T., A. Bruhn, N. Papenberg, and J. Weickert. High Accuracy Optical Flow Estimation Based on a Theory for Warping. in Computer Vision - ECCV 2004. 2004. Berlin, Heidelberg: Springer Berlin Heidelberg.

34. Weinzaepfel, P.a.R., Jerome and Harchaoui, Zaid and Schmid, Cordelia, DeepFlow: Large Displacement Optical Flow with Deep Matching, in Proceedings of the IEEE International Conference on Computer Vision (ICCV). 2013.

35. Revaud, J.a.W., Philippe and Harchaoui, Zaid and Schmid, Cordelia, EpicFlow: Edge-Preserving Interpolation of Correspondences for Optical Flow, in Proceedings of the IEEE Conference on Computer Vision and Pattern Recognition (CVPR). 2015.

36. Shah, S.T.H. and X. Xuezhi, Traditional and modern strategies for optical flow: an investigation. SN Applied Sciences, 2021. 3(3): p. 289.

37. Ronneberger, O., P. Fischer, and T. Brox. U-Net: Convolutional Networks for Biomedical

Image Segmentation. in Medical Image Computing and Computer-Assisted Intervention – MICCAI 2015. 2015. Cham: Springer International Publishing.

38. Hui, T.-W.a.T., Xiaoou and Loy, Chen Change, LiteFlowNet: A Lightweight Convolutional Neural Network for Optical Flow Estimation, in Proceedings of the IEEE Conference on Computer Vision and Pattern Recognition (CVPR). 2018.

39. Ranjan, A.a.B., Michael J., Optical Flow Estimation Using a Spatial Pyramid Network, in Proceedings of the IEEE Conference on Computer Vision and Pattern Recognition (CVPR). 2017.

8 CONTACT

Corresponding author: Qiang Cheng

Email: qiang.cheng@aalto.fi

Address: Puumiehenkuja 5A, Espoo Finland